Order online now!

www.rockland.com
tech@rockland.com
+1 484.791.3823

Datasheet for 600-401-104-0.1

Collagen Type II Antibody

Overview

Description:	Anti-Collagen Type II (RABBIT) Antibody - 600-401-104-0.1
Item No.:	600-401-104-0.1
Size:	100 µg
Applications:	Dot Blot, IHC, IF, Multiplex, WB
Reactivity:	Human, Bovine
Host Species:	Rabbit

Product Details

Background:	Rockland produces highly active antibodies and conjugates to collagens. Collagens are highly conserved throughout evolution and are characterized by an uninterrupted ''Glycine-X-Y'' triplet repeat that is a necessary part of the triple helical structure. For these reasons, it is often extremely difficult to generate antibodies with specificities to collagens. The development of 'type' specific antibodies is dependent on NON-DENATURED three-dimensional epitopes. Rockland extensively purifies collagens for immunization from human and bovine placenta and cartilage by limited pepsin digestion and selective salt precipitation. This preparation results in a native conformation of the protein. Antibodies are isolated from rabbit antiserum and are extensively cross-adsorbed by immunoaffinity purification to produce 'type' specific antibodies. Greatly diminished reactivity and selectivity of these antibodies will result if denaturing and reducing conditions are used for SDS-PAGE and immunoblotting. Ideal for investigators involved in Cell Biology, Signal Transduction and Stem Cell research.
Synonyms:	rabbit anti-Collagen Type II antibody, Collagen alpha-1 (II) chain, Alpha-1 type II collagen, Cartilage collagen antibody, Chondrocalcin antibody, COL2A1 antibody
Host Species:	Rabbit
Clonality:	Polyclonal
Format:	IgG

Target Details

Gene Name:	COL2A1
Reactivity:	Human, Bovine

Immunogen Type:	Native Protein
Immunogen:	Collagen Type II from human knee cartilage and bovine nasal cartilage.
Purity/Specificity:	Collagen II Antibody has been prepared by immunoaffinity chromatography using immobilized antigens followed by extensive cross-adsorption against other collagens. Some class specific anti-collagens may be specific for three-dimensional epitopes which may result in diminished reactivity with denatured collagen or formalin-fixed, paraffin embedded tissues. This antibody reacts with most mammalian Type II collagens and has expected cross-reactivity with Type IV and VI and negligible cross reactivity to Type I, III and V collagens. Non-specific cross reaction of anti-collagen antibodies with other human serum proteins or non-collagen extracellular matrix proteins has not been tested.
Relevant Links:	• Anti-Collagen IHC protocol • UniProtKB - P02458 • NCBI - NP_001835.3 • GeneID - 1280

Application Details

Tested Applications:	Dot Blot, IHC
Suggested Applications:	IF, Multiplex, WB (Based on references)
Application Note:	Anti-Collagen Type II has been tested by dot blot and IHC and is suitable for indirect trapping ELISA for quantitation of antigen in serum using a standard curve, immunoprecipitation, immunohistochemistry, native (non-denaturing, non-dissociating) PAGE, and western blotting for highly sensitive qualitative analysis.
Assay Dilutions:	All assays should be optimized by the user. Recommended dilutions (if any) may be listed below.
ELISA:	1:5,000 - 1:50,000
FLISA:	1:100
IF:	User Optimized
IHC:	1:50 - 1:200
IP:	1:100
WB:	1:1,000 - 1:10,000

Formulation

Physical State:	Liquid (sterile filtered)

Concentration:	1.15 mg/mL by UV absorbance at 280 nm
Buffer:	0.02 M Potassium Phosphate, 0.15 M Sodium Chloride, pH 7.2
Preservative:	0.01% (w/v) Sodium Azide
Stabilizer:	None

Shipping & Handling

Shipping Condition:	Wet Ice
Storage Condition:	Store vial at 4° C prior to opening. This product is stable at 4° C as an undiluted liquid. Dilute only prior to immediate use. For extended storage, mix with an equal volume of glycerol, aliquot contents and freeze at -20° C or below. Avoid cycles of freezing and thawing.
Expiration:	Expiration date is one (1) year from date of receipt.

Images

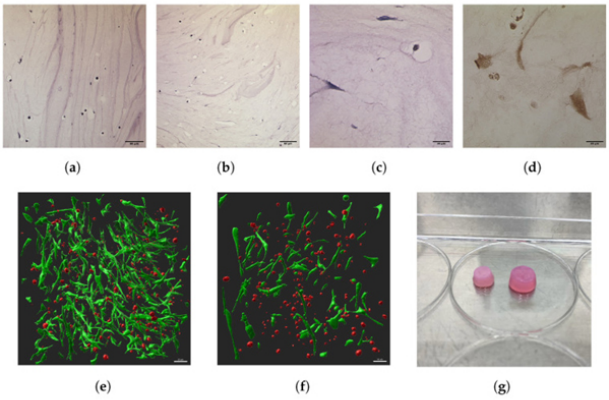

Immunohistochemistry
(a–d) Show photos of histological sections. (a,b) HE stainings of D4 at 10×: (a) is the control, (b) is the ES group. (c) An HE staining of the D7 ES group at 40×; (d) a COL2 immunohistochemical staining from the D10 ES group at 40× magnification. (e,f) Show 3D renderings of stacks from two-photon imaging from D7. (e) Displays the ES group; (f) the control group. (g) Shows a physical image of the scaffolds at D10. The left scaffold is from the ES group, the right scaffold is from the control group. Fig 3.
PMID: 38927763

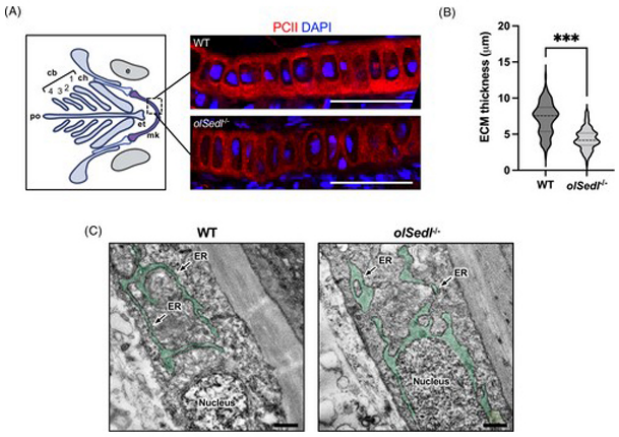

Immunofluorescence Microscopy

Col2 expression and secretion is compromised in olSedl−/− fish. (A) Representative immunostaining of Meckel's cartilage (boxed area in the graphic representation on the left) of WT and olSedl−/− fish showing a reduction in type II collagen (red) levels. Nuclei are counterstained with DAPI (blue) [(cb1-4) ceratobranchial pairs 1 to 4, (ch) ceratohyal, (et) ethmoid plate, (mk) Meckel's cartilage, (po) posterior limit, (e) eye]. (B) Quantification of ECM thickness in WT and olSedl−/− fish. (C) Representative electron microscopy images (16× magnification) of a vertebral section of stage 40 WT and olSedl−/− fish. The ER is pseudocolored in green and the ER cisternae are indicated by black arrows. The dashed line and punctate pattern in the violin plot in (B) show the median and quartiles, respectively. (B): n > 90 measurements. ***p < 0.001, two-tailed unpaired t-test with Welch's correction. Scale bar in (A): 30 µm, (C): 500 nm. Fig 2. PMID: 37963679

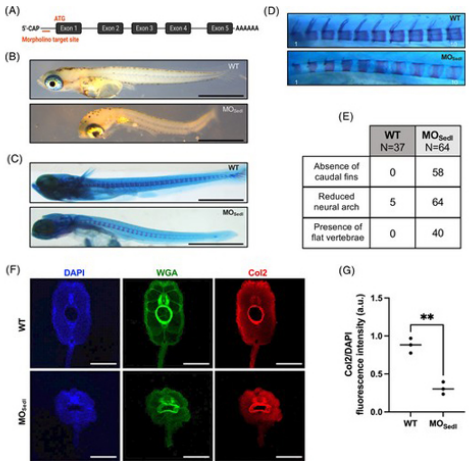

Immunofluorescence Microscopy

olSedl morpholino fish manifest a SEDT-like phenotype. (A) Schematic representation of the morpholino targeting site at the ATG in exon 1 of olSedl. (B) Representative brightfield images of WT and MOSedl fish. (C) Representative whole-mount alcian blue-alizarin red staining images showing that MOSedl lack cartilaginous intermediates in the caudal fin and have a reduced number of vertebrae. (D) High magnification alcian blue-alizarin red staining from the first to tenth vertebra showing altered morphology. (E) Quantification of the observed phenotypes. (F) Immunofluorescence analysis of WT and MOSedl sections of frontal vertebra showing a significant alteration in size and morphology. Nuclei are counterstained with DAPI (blue), connective tissue is visualized with fluorescent Wheat Germ Agglutinin (WGA, green), while type II collagen (Col2) is shown in red. (G) Col2 fluorescence intensity measurement of WT and MOSedl sections of frontal vertebra; N = 3, median is indicated. **p = 0.001, two-tailed unpaired t-test. Scale bar in (B) and (C): 1 mm; (F): 100 µm. Fig 3. PMID: 37963679

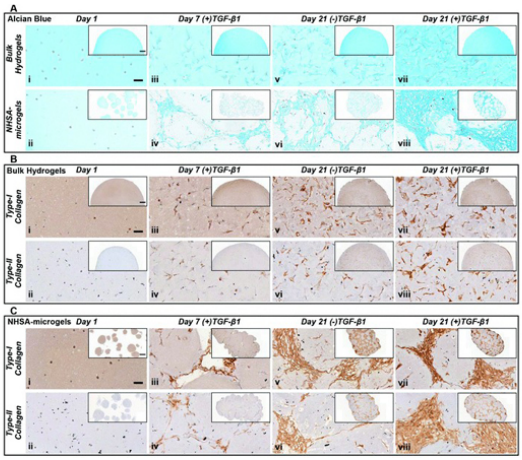

Immunohistochemistry

Histological characterisation of bulk hydrogels and NHSA-microgels at day 1, 7 & 21 of in vitro culture. (A) Alcian blue (pH 1) staining – bulk hydrogel (top row) & NHSA-microgels (bottom row). (B) Type-I and type-II collagen immunohistochemical staining on bulk hydrogels. (C) Type-I and type-II collagen immunohistochemical staining on NHSA-microgels (scale bar: 50 µm/inset: 500 µm). Fig 5. PMID: 31994552

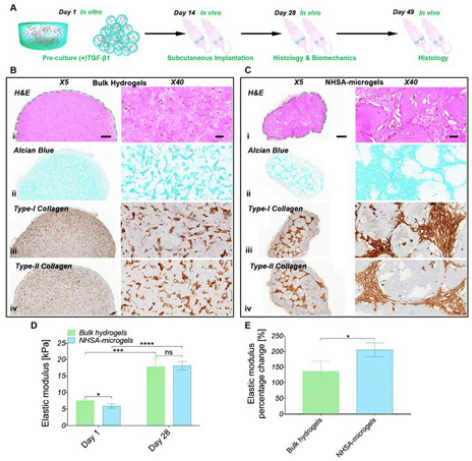

Immunohistochemistry

(A) Schematic representation of hCC-laden bulk hydrogels and NHSA-microgel in vivo chondrogenesis: after in vitro pre-culture in chondrogenic media ((+)TGF-β1) for two weeks, samples were subcutaneously implanted into nude mice (left mice – bulk hydrogel; right mice – NHSA-microgels) and maintained in vivo for an additional two weeks (day 28) or five weeks (day 49). (B) Histological analysis of bulk hydrogel at day 28 (i: H&E, ii: Alcian blue, iii: type-I collagen, iv: type-II collagen). (C) Histological analysis of NHSA-microgel at day 28 (i: H&E, ii: Alcian blue, iii: type-I collagen, iv: type-II collagen) (scale bar: X5/500 µm; X40/50 µm). (D) Nanoindentation tests at day 1 and day 28. (E) Percentage elastic modulus increment profile showing hCC-laden bulk hydrogel and NHSA-microgel mechanical properties enhancement after 28 days maintenance in vivo (*P < 0.05, **P < 0.01, ***P < 0.001, and ****P < 0.0001). Fig 7. PMID: 31994552

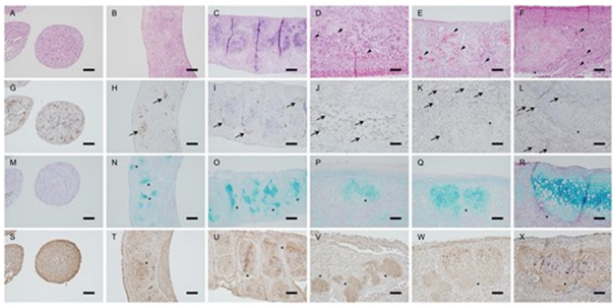

Immunohistochemistry
Histological findings of the spheroids, artificial tracheas and transplanted grafts. (A–F) Haematoxylin and eosin staining, (G–L) immunohistochemical staining with anti-CD31 antibodies, (M–R) Alcian blue staining and (S–X) immunohistochemical staining with anti-collagen II antibodies. (A, G, M and S) Spheroids; (B, H, N and T) bio-3D-printed artificial tracheas after maturation; (C, I, O and U) Day 1; (D, J, P and V) Day 8; (E, K, Q and W) Day 11 and (F, L, R and X) Day 23. Cartilage tissue can be observed in artificial tracheas after maturation and maintained over 10 days (asterisk). Capillary-like tubes consisting of CD31-positive cells (arrow) can be seen in artificial tracheas after maturation. Red blood cells are observed from Day 8 in the capillary-like tube formations (arrowhead). Scale bar = 100µm. Fig 5. PMID: 29346562

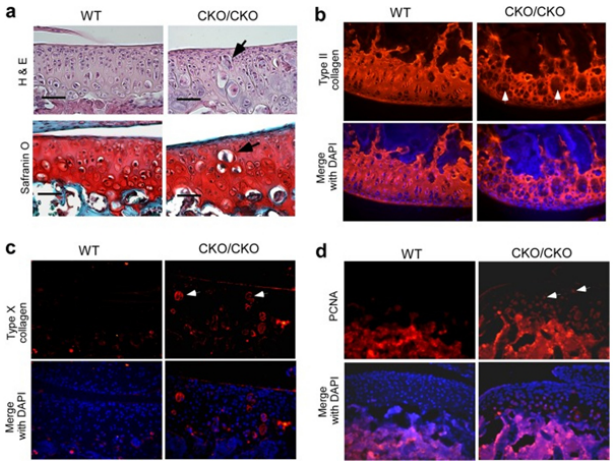

Immunofluorescence Microscopy
Articular chondrocyte hypertrophy and proliferation in 1-month-old ESET-null mice. a, 1-month-old knee joints were stained by H&E and Safranin O for detailed morphological analysis. b, 1-month-old knee sections were stained with an anti-type II collagen antibody. The type II collagen network was stained red, and nuclei were stained blue by DAPI. c, anti-type X collagen antibody specifically stains hypertrophic chondrocytes (red) in 1-month-old knee sections. d, anti-PCNA antibody detects cells positive for the proliferation marker in 1-month-old knee sections. Arrows in a–d indicate locations of hypertrophic or proliferative chondrocytes near the superficial zone in ESET-null mice. A total of three wild-type and five knock-out mice were examined, and images from representative experiments are shown. Genotypes of the mice are indicated on the top. Scale bar: 50 µm. Fig 3. PMID: 24056368

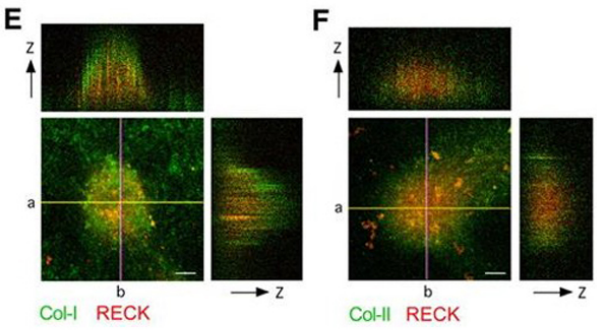

Immunofluorescence Microscopy
(E and F) Localization of type I and type II collagen at cartilaginous nodules formed by ATDC5 cells. ATDC5 cells incubated for 15 days were fixed and stained with anti-RECK (red) plus anti-type I collagen (green; E) or anti-RECK (red) plus anti-type II collagen (green; F). Reconstituted z-axis images along two cutting lines (a,b) are shown in the top and right panels, respectively. Bars, 100 µm in E,F. Fig 2.
PMID: 17298979

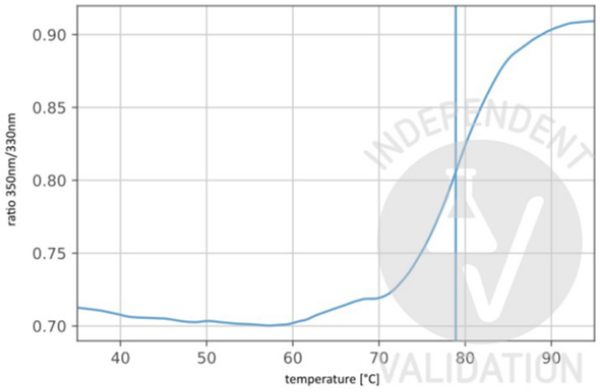

Figure
Unfolding profile of Anti-Collagen Type II (RABBIT) Antibody (p/n 600-401-104). The fluorescence signal is plotted against temperature. The vertical line indicates the Ti at 78.9°C. Independently Validated by antibodies-online GmbH (p/n ABIN7565872/ ABIN5596824/ ABIN5596825) courtesy of NanoTemper Technologies.

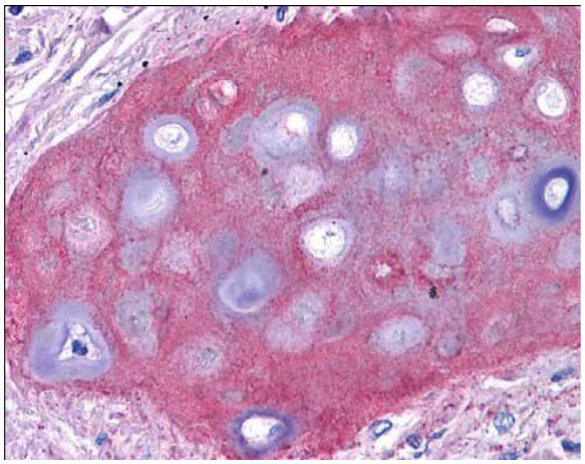

Immunohistochemistry
Rockland anti collagen II antibody (600-401-104 Lot 26014, 1:400, 45 min RT) showed moderate staining of in FFPE human bronchiolar cartilage (shown in image). Though not shown, faint to moderate staining of tonsillar squamous epithelium, prostatic stroma, breast, colon, placenta, and dermal connective tissues was also observed. All other tissues, including brain, breast epithelium, colon epithelium, heart, intestine, kidney, liver, lung, skeletal muscle, pancreas, spleen, testis, thymus, thyroid, and uterus were negative for staining Slides were steamed in 0.01 M sodium citrate buffer, pH 6.0 at 99-100°C - 20 minutes for antigen retrieval. Image provided courtesy of LifeSpan Biosciences, Seattle, WA

References

- Lehmenkotter N et al. Electrical Stimulation of Mesenchymal Stem Cells as a Tool for Proliferation and Differentiation in Cartilage Tissue Engineering: A Scaffold-Based Approach. *Bioengineering (Basel).* (2024)
- Zappa F et al. Role of trafficking protein particle complex 2 in medaka development. *Traffic.* (2024)
- Li F et al. Microencapsulation improves chondrogenesis in vitro and cartilaginous matrix stability in vivo compared to bulk encapsulation. *Biomed Mater. Sci.* (2020)
- Levinson C et al. Is there a scientific rationale for the refixation of delaminated chondral flaps in femoroacetabular impingement? a laboratory study. *Clin Orthop Relat Res.* (2020)
- Ozturk E et al. Tyrosinase-crosslinked, tissue adhesive and biomimetic alginate sulfate hydrogels for cartilage repair. *Biomed Mater.* (2020)
- Unlu G, Qi X, Gamazon ER, et al. Phenome-based approach identifies RIC1-linked Mendelian syndrome through zebrafish models, biobank associations and clinical studies. *Nat Med.* (2020)
- Lee M, Bae K, Levinson C, Zenobi-Wong M. Nanocomposite bioink exploits dynamic covalent bonds between nanoparticles and polysaccharides for precision bioprinting. *Biofabrication.* (2020)
- Taniguchi D, Matsumoto K, Machino R, et al. Human lung microvascular endothelial cells as potential alternatives to human umbilical vein endothelial cells in bio-3D-printed trachea-like structures. *Tissue Cell.* (2020)
- Cavalli E, Levinson C, Hertl M, et al. Characterization of polydactyly chondrocytes and their use in cartilage engineering. *Sci Rep.* (2019)
- Levinson C, Cavalli E, Sindi DM, et al. Chondrocytes From Device-Minced Articular Cartilage Show Potent Outgrowth Into Fibrin and Collagen Hydrogels. *Orthop J Sports Med.* (2019)
- Levinson C, Lee M, Applegate LA, Zenobi-Wong M. An injectable heparin-conjugated hyaluronan scaffold for local delivery of transforming growth factor β1 promotes successful chondrogenesis. *Acta Biomater.* (2019)
- Forrester A, De Leonibus C, Grumati P, et al. A selective ER-phagy exerts procollagen quality control via a Calnexin-FAM134B complex. *EMBO J.* (2019)
- Schuelke J, Meyers N, Reitmaier S, Klose S, Ignatius A, Claes L. Intramembranous bone formation after callus distraction is augmented by increasing axial compressive strain. *PLoS One.* (2018)
- EmmaCavalli et al. A comparative study of cartilage engineered constructs in immunocompromised, humanized and immunocompetent mice. *Journal of Immunology and Regenerative Medicine* (2018)
- Taniguchi D et al. Scaffold-free trachea regeneration by tissue engineering with bio-3D printing. *Inetact Cardiovasc Thorac Surg.* (2018)
- Formica FA et al. Cell-Instructive Alginate Hydrogels Targeting RhoA. *Bioconjug Chem.* (2018)
- Morgese G et al. Nanoassemblies of tissue-reactive, polyoxazoline graft-copolymers restore the lubrication properties of degraded cartilage. *ACS Nano.* (2017)
- He et al. Repair of osteochondral defects with in vitro engineered cartilage based on autologous bone marrow stromal cells in a swine model. *Scientific Reports* (2017)
- Formica FA, Öztürk E, Hess SC, et al. A Bioinspired Ultraporous Nanofiber-Hydrogel Mimic of the Cartilage Extracellular Matrix. *Adv Healthc Mater.* (2016)

- Nicolas Broguiere et al. Factor XIII Cross-Linked Hyaluronan Hydrogels for Cartilage Tissue Engineering. *ACS Biomater. Sci. Eng.* (2016)
- Broguiere N et al. Factor XIII cross-linked hyaluronan hydrogels for cartilage tissue engineering. *ACS Biomater Sci Eng.* (2016)
- Liedert, A et al. Osteoblast-specific Krm2 overexpression and Lrp5 deficiency have different effects on fracture healing in mice. *PloS One* (2014)
- Martins EA, Michelacci YM, Baccarin RY, Cogliati B, Silva LC. Evaluation of chitosan-GP hydrogel biocompatibility in osteochondral defects: an experimental approach. *BMC Vet Res.* (2014)
- Rojewski MT, Fekete N, Baila S, et al. GMP-compliant isolation and expansion of bone marrow-derived MSCs in the closed, automated device quantum cell expansion system. *Cell Transplant.* (2013)
- View More ...

Disclaimer